Neoplasma 2023; 70(4): 555–565

doi:10.4149/neo_2023_230317N150

Hydrogel-based miR-192 delivery inhibits the development of hepatocellular carcinoma by suppressing the GSK3β/Wnt/β-catenin pathway

Qing YANG[1,#], Xiaojv ZHUGE[1,#], Weili LIN[2], Weilai YU[1], Yu ZHU[2], Changsheng SHI[3,*], Zhengchao SHI[1,*]

[1]Department of Gastroenterology, The Third Affiliated Hospital of Wenzhou Medical University, Rui'an, Wenzhou, China; [2]Ultrasound Room, The Third Affiliated Hospital of Wenzhou Medical University, Rui'an, Wenzhou, China; [3]Department of Interventional Vascular Surgery, The Third Affiliated Hospital of Wenzhou Medical University, Rui'an, Wenzhou, China

**Correspondence: shichangsheng85@163.com; ymszc@126.com*
[#]Contributed equally to this work.

Received March 17, 2023 / Accepted August 24, 2023

Hepatocellular carcinoma (HCC) is a primary liver cancer characterized by high invasiveness, metastasis, and poor prognosis, which lacks effective treatments. Although the role of miR-192 in HCC development has been recognized, the underlying molecular mechanism is still poorly understood. This study aimed to explore the impact of mir-192 on HCC and its potential as a therapeutic strategy. Wound healing assay, Transwell assay, CCK-8 assay, and flow cytometry were performed to detect the impact of miR-192 on HCC cell metastasis, invasion, proliferation, and apoptosis, respectively. q-PCR and western blot were applied to measure the relative mRNA and protein expression of the GSK3β/Wnt/β-catenin pathway in miR-192-overexpressing cell lines. Immunofluorescence was carried out to detect the nuclear translocation of β-catenin. starBase website and dual luciferase reporter assay were used to verify the interaction between miR-192 and the target gene WNT10B 3'-untranslated region (3'-UTR) of the Wnt pathway. In addition, we developed algin/polyethyleneimine@miR-192 (AG/PEI@miR-192) nanohydrogel for *in vivo* delivery of miR-192-agomir. The results revealed that overexpressed miR-192 reduced the expression of HCC cell surface markers CD90, EpCAM, and CD133. Moreover, miR-192 overexpression inhibited HCC cell metastasis, invasion, and proliferation, promoted cell apoptosis, and reduced GSK3β/Wnt/β-catenin pathway expression. Additionally, AG/PEI@miR-192 exhibited good drug release and tumor inhibition. In conclusion, our study suggested that miR-192 inhibits HCC development by suppressing the GSK3β/Wnt/β-catenin pathway and proposed a promising hydrogel-based miR-192 delivery approach to hinder tumor growth.

Key words: hepatocellular carcinoma; miRNA; hydrogel-based delivery; GSK3β; Wnt; β-catenin

Primary liver cancer is currently one of the top four death-lead cancers worldwide, and its incidence and mortality rates increase year by year, with a 5-year survival rate of only 18%, posing a serious threat to people's lives and health [1]. Hepatocellular carcinoma (HCC) accounts for about 80% of the total incidence of primary liver cancer, characterized by high invasiveness, easy metastasis, and poor prognosis [2], making clinical treatment difficult. Despite surgical resection remains the most effective approach of various treatment options, the lack of typical clinical symptoms in the early stage of HCC often leads to delayed diagnosis, and even after surgery, the 5-year survival rate of patients is still very low [3]. At present, drugs such as sorafenib, Regorafenib, lenvatinib, and PD-1 antibodies are clinically developed and used, but their effectiveness remains limited. As a result, there is still a lack of effective treatment for HCC, which is due to the unclear understanding of the mechanisms regulating the pathogenesis [4]. Therefore, it is important to identify more mechanisms of HCC pathogenesis to provide more therapeutic approaches and therapeutic targets for timely detection as well as for the treatment of HCC.

At present, a large number of surface markers of liver tumor cells have been found to regulate the characteristics of liver cancer cells. Among them, EpCAM has been found to activate the Wnt signaling pathway, thereby regulating the characteristics of hepatocellular carcinoma cells [5]. Also, Wnt/β-catenin, AKT, and TGF-β signaling pathways are aberrantly expressed in liver tumor stem cells [5]. Besides, GSK3 is a key signaling molecule in cancer and Wnt/β-catenin and has a role in inhibiting or activating signaling

nodes of control molecules, such as c-Myc and P53 [6]. As an important metabolic organ, the liver plays an essential role in glucose and lipid metabolism. Previous research indicated that HCC cells are associated with a series of metabolic imbalances, including alterations in glycolysis [3, 7]. Therefore, targeting glycolysis has a certain inhibitory effect on HCC cells.

miRNA is a short non-coding RNA with a length of about 21–23 nt, which exerts its regulatory ability mainly by mediating miRNA adenylation or hindering its translation [8]. miRNAs play a crucial regulatory role in the Warburg effect by directly or indirectly modulating key enzymes involved in glycolysis through the regulation of oncogene expression levels or participation in cancer-related pathways, ultimately influencing the progression of HCC [9]. For example, miR-365a increases aerobic glycolysis and promotes HCC cell proliferation [10], while, miR-139-5p inhibits aerobic glycolysis, as well as cell proliferation, migration, and invasion in HCC [11]. miR-192-5p (miR-192) is the second most abundant miRNA in the liver and is often silenced in many liver cancer cells with positive liver tumor stem cell markers, such as EpCAM, CD90, and CD133 [12, 13]. It was shown that miR-192 deletion enhanced the expression of the glycolytic-related genes Pfkfb3, Glut1, and c-Myc, facilitating tumor cell growth and tumor stemness. And c-Myc was shown to directly inhibit miR-192 transcription level, manifested as high glycolysis level in HCC cells, which is a critical part of liver cancer development [14, 15].

It has been shown that GSK3/Wnt/β-catenin/c-Myc/miR-192 plays an important role in hepatocarcinogenesis. However, their regulatory roles and interrelationships in the regulation of hepatocarcinogenesis have not been reported. Additionally, although clinical guidelines strongly recommend multidisciplinary strategies for the treatment of HCC, the choice of materials and therapeutic approaches is limited [16]. Qu et al. [17] found that injectable hydrogels with pH responsiveness and self-healing ability have great potential for anticancer drug delivery. Yan et al. [16] reported that an in situ thermal-responsive magnetic hydrogel could lead to the effective multidisciplinary treatment of HCC and reduce postoperative recurrence. Thus, this study hypothesized that miR-192 inhibits HCC by regulating the GSK3/Wnt/β-catenin/c-Myc signaling pathway, and develops AG/PEI nanohydrogel to deliver miR-192, providing a reference for clinical drug development.

Materials and methods

Cell culture and transfection. Normal human liver cell line (LO2) and two HCC cell lines (Bel-7402, HepG2) were purchased from Procell (Wuhan, China). Next, they were maintained in DMEM (Gibco, USA) with 10% fetal bovine serum (Gibco, USA) and 1% penicillin/streptomycin (Gibco, USA) at 37 °C in 5% CO_2.

For overexpression of miR-192, these cells were transfected with miR-192 mimic (5'-ucugcuccgugucuucacuccc-3') and negative control (5'-uucgcuccguauccucacucgc-3') using the Lipo8000™ transfection reagent (Beyotime Biotechnology, Shanghai, China) according to the manufacturer's protocol.

Quantitative real-time PCR (qRT-PCR). Total RNA from cells was extracted using the TRIzol reagent (Invitrogen) following the manufacturer's protocol. Then, total RNA was reverse transcribed into cDNA using the RNA cDNA first strand synthesis kit (TransGen Biotech, Beijing, China). Next, the cDNA was amplified using the Ex Taq™-kit (TAKARA) for qRT-PCR. The $2^{\Delta\Delta CT}$ method was applied to analyze relative RNA expression. The primers were as follows: GAPDH-F 5'-AGGCCGGTGCTGAGTATGTC-3'; GAPDH-R 5'-TGCCTGCTTCACCACCTTCT-3'; GSK3β-F 5'-GGCAGCATGAAAGTTAGCAGA-3'; GSK3β-R 5'-GGCGACCAGTTCTCCTGAATC-3'; β-catenin-F 5'-GAGCCGTCAGTGCAGGAG-3'; β-catenin-R 5'-CAGCTTGAGTAGCCATTGTCC-3'; c-Myc-F 5'-CGTTGGAAACCCCGCAGACA-3';c-Myc-R5'-GATATCCTCACTGGGCGCGG-3'.

Flow cytometry. The FITC Annexin V Apoptosis Detection Kit I (556547, BD Pharmingen) was applied to perform flow cytometry. Cells were washed twice with cold PBS and resuspended at a concentration of 1×10^6 cells/ml in 1× binding buffer. Next, 100 μl of the cell suspension (1×10^5 cells) was transferred into a 5 ml culture tube, followed by the addition of 5 μl FITC Annexin V and 5 μl PI. After that, the cells were gently vortexed and incubated for 15 min in the dark at room temperature (25 °C). 400 μl of 1× binding buffer was added to each tube and analyzed using the CytoFLEX flow cytometer (Beckman Coulter) within 1 h.

Flow cytometry was also employed to detect the expression of CD90, EpCAM, and CD133 [18]. Briefly, after reaching 90% confluence, CD90-PE antibody (5E01), CD133-APC (W6B3C1), and EpCAM-FITC (9C4) (all from BioLegend) were applied. Data were evaluated using the CytoFLEX flow cytometer.

Wound-healing assay. A wound-healing assay was performed to detect the migration abilities of the cells. Horizontal lines were drawn evenly across the back of the 6-well plate using a marker pen, approximately one line every 0.5 to 1 cm, each well was crossed by at least 5 lines. The cells were seeded into 6-well plates. The wound was created using the tip of the gun to scratch perpendicular to the horizontal line. Next, cells were washed three times with PBS, the scratched-down cells were removed and added to the serum-free medium to minimize the impact of cell proliferation. Then, they were placed in an incubator at 37 °C with 5% CO_2. Samples were taken and photographed at 0 and 24 h.

Transwell assay. The invasion and migration abilities of these cells were determined by Transwell assay. DMEM high sugar culture medium (Hyclone) containing 10% fetal bovine serum (Gibco) and 1% double antibiotics (mixed solution of penicillin and streptomycin) were used to culture

cells at 37 °C in an incubator (Thermo) with 5% CO_2. The cells were observed as adherent cells under the microscope (Shanghai Caikang Optical Instrument Co., Ltd., Shanghai, Chian). Before the experiment, the Matrigel stored at –20 °C was transferred to the refrigerator at 4 °C, melted overnight, and diluted (serum-free medium: matrix gel=2:1). To enhance the invasion and migration, twenty-four hours before the experiment, the cells in different groups after transfection were replaced with serum-free basic medium to continue the culture. Next, 24-well plates and Transwell chambers (COSTAR) were soaked in 1× PBS for 5 min 24 h before the assay. 80 μl of Matrigel (Corning) was spread in the chamber and placed in a 37 °C incubator for 30 min to solidify. After digestion with trypsin, cells were washed with a serum-free medium, resuspended in a medium containing 1% FBS, counted, diluted to 3×10^5 cells/ml, and inoculated into Transwell chambers, with 0.3 ml of cell suspension per chamber and 0.7 ml of a complete culture medium containing 10% FBS in the lower 24-well plate, with 3 replicate wells/group. The chamber was then put in the 37 °C incubator for 48 h, followed by the addition of 1 ml of 4% formaldehyde solution per well, and fixation for 10 min at room temperature. Next, the fixation solution was removed and washed with 1× PBS once. 1 ml of 0.5% crystal violet solution (Solarbio) was added to each well. After staining for 30 min, it was washed three times with 1× PBS and dried. The cells without migration/invasion in the Transwell chamber were carefully wiped with a cotton swab and observed under a 200× microscope to count the number of cells in each field of view.

CCK-8 assay. After Bel-7402 and HepG2 cells were transfected with or without miR-192 mimic, they were seeded in 96-well plates (Corning) at 1,000 cells/well. Then, 10 μl of the CCK-8 kit (BBI Life Sciences) was added to each well, and the plates were cultivated in a cell incubator (Thermo) at 37 °C for 1 h protected from light. The absorbance value at 450 nm was measured by an enzyme calibration.

Western blot. Protein was extracted by RIPA lysis buffer (Beyotime, Shanghai, China) and quantified with a BCA protein concentration assay kit (Beyotime, Shanghai, China). 20 μg of proteins were separated via sodium dodecyl sulfate-polyacrylamide gel electrophoresis and transferred to PVDF membranes. After blocking in TBST with 5% skimmed milk powder, the membranes were incubated with primary antibodies (GSK3β, 22104-1-AP; p-GSK3β, 67558-1-Ig; β-catenin, 51067-2-AP; c-Myc, 10828-1-AP; Tcf7, 14464-1-AP; Lef1,14972-1-AP; Proteintech), followed by washing with TBST 5 to 6 times (5 min/time). Then, the membranes were incubated with a secondary antibody (HRP-conjugated Affinipure Goat Anti-Rabbit IgG(H+L), SA00001-2; Proteintech) and washed with TBST 5 to 6 times (5 min/time). The protein blots were visualized using the ECL plus kit (Beyotime) and quantified using ImageJ.

Immunofluorescence staining. The experimental group was transfected with miRNA-192 mimic, while the control group received no treatment. After 48 h of transfection, the cells were fixed with 4% paraformaldehyde for 15 min. Then, the cells were washed twice with PBS and incubated with 0.2% Triton X-100 diluted in PBS for 10 min to achieve permeabilization. Subsequently, the cells were incubated with an anti-β-catenin antibody (1:200; Cell Signaling Technology, #8480) overnight at 4 °C in the dark. On the following day, the cells were washed with PBS and incubated with an anti-rabbit secondary antibody (Alexa Fluor 488 conjugated; 1:500; Cell Signaling Technology, #4412) at room temperature in the dark for 1 h. All images were captured using a Leica confocal microscope. In the immunofluorescence experiment aimed at observing the delivery efficiency of the hydrogel, the prepared FITC was directly incubated with cells for 2 or 6 h, referred to as the free FITC group. The FITC was incorporated into the hydrogel (using the same method as the miR-192-incorporated hydrogel, final concentration 15 mM) and co-cultured with cells in 10% fetal bovine serum for 2 or 6 h, referred to as the AG/PEI@FITC group. Finally, the delivery effect of the hydrogel was assessed by observing the localization and intensity of fluorescence signals.

Dual-luciferase reporter assay. The wild-type sequence of WNT10B 3'-untranslated region (3'-UTR) containing miR-192-binding site was inserted into the luciferase reporter vector to generate the luciferase reporter plasmid (WNT10B-WT). Next, the miR-192-binding site was mutated to construct the mutant-type luciferase reporter plasmid (WNT10B-MUT). The constructed luciferase reporter plasmid together with miR-192 mimic or miR-NC were transfected into Bel-7402 and HepG2 cells. After that, a dual-luciferase reporter gene assay kit (Yeasen Biotechnology) was employed to measure the luciferase activity.

Hydrogel preparation. Sodium alginate powder was dissolved in ultrapure water to obtain an algin (AG) water solution (1% wt). 3 ml AG water solution and 8.25 mg 1-ethyl-3-(3-dimethyl aminopropyl)-carbodiimide (EDC) was added to a reaction bottle, followed by magnetic stirring for 3 h to activate the carboxyl group on the surface of sodium alginate. Then, the activated solution was added to the dichloromethane (DCM) solution containing sodium dioctyl sulfosuccinate (AOT) (2.5% wt, 6 ml) drop by drop under magnetic stirring (1,000 × g, 5 min). Many oil droplets were formed in the solution during the dropping process. After the oil droplets were stirred evenly with the solution, a water-in-oil (W/O) emulsion was initially formed. The W/O emulsion was slowly added dropwise to an ultrapure water solution containing polyvinyl alcohol (PVA, 2% wt, 45 ml) and magnetically stirred (1,000×g, 10 min) until a polymer emulsion of water-in-oil water (W/O/W) was generated. Next, an ultrapure water solution containing polyethyleneimine (PEI) was slowly added drop by drop to the formed emulsion, and the mixture was magnetically stirred for 24 h. The organic solvent was removed by evaporation, followed by centrifugation (8,000×g), and the supernatant was discarded. Then, purification with ultrapure water was performed three

times to remove excess reactants and by-products to obtain AG/PEI nanohydrogel. The miR-192-agomir, which has superior transfection characteristics compared to miR-192-mimics and does not require transfection reagents, was dissolved in sterile diethyl pyrocarbonate water and vortexed with AG/PEI nanohydrogels for 1 min and incubated for 1 h at room temperature to form miRNA-loaded nanohydrogel particles with a miR-192-agomir concentration of 5 μM.

Characterizations of AG/PEI hydrogel nanoparticles. The AG/PEI nanohydrogel was left for 2, 4, or 6 months to observe the precipitation and color. Nanoparticle tracking analysis (NTA) was performed to detect the nanoparticles of AG/PEI hydrogel. The real-time image of the scattered light of the nanoparticles was captured by the LM20 nanoparticle tracking analyzer (NanoSight, UK) through a fixed-wavelength laser with a wavelength of 635 nm and a CCD (charge-coupled device) camera with a certain magnification. The Brownian motions of the particles make the scattered light point move randomly in the monitoring field of view. The center position and movement speed of the scattered light point can accurately reflect the particle position and movement speed. Therefore, the motion trajectory of each scattered light point identified by the nanoparticle tracking analysis 2.3 software (NTA2.3 software, NanoSight, UK) is the Brownian motion trajectory, and then the particle size is calculated by the Stokes-Einstein formula.

Scanning electron microscope analysis. A scanning electron microscope (HITACHI, Japan) was applied to observe the morphology and particle size of the AG/PEI@miR-192 nanohydrogel. A small amount of lyophilized nanohydrogel powder was placed on the sample stage. Next, the ion sputtering was performed under a vacuum (10 Pa), with a current of 15 mA and a coating time of 130 s. The thickness of the coating was 10 nm, and the distance between the sample stage and the gold target was 5 cm.

Drug release of AG/PEI@miR-192 nanohydrogel. The release characteristics of AG/PEI@miR-192 were determined using the high-performance liquid chromatography (HPLC) method. The prepared AG/PEI@miR-192 and miR-192 were configured with buffer to solutions with a concentration of 1 mg/ml, respectively. 1 ml of AG/PEI@miR-192 and 1 ml of miR-192 solution were placed in a dialysis bag with a molecular weight cut-off of 8000-10000. Then, the dialysis bag was put in a container with 9 ml buffer solution and shaken in a shaker at 37 °C. Samples were taken at different time points (0, 1, 2,5, 12, 24, 36, 48, 72, 96, and 120 h), 1 ml of solution was taken from outside of the dialysis bag, and the container was replenished with the corresponding buffer solution. The concentration of the liquid removed at different time points was measured by the HPLC (Agilent 1260). Then the drug release curve was plotted. Calculation method: The standard curve is generated by correlating the drug concentration with the corresponding peak area measured by HPLC. The peak area of the sample is then substituted into the established standard curve to determine the drug concentration.

Animal experiments. The animal study was approved by the Ethics Committee of The Third Affiliated Hospital of Wenzhou Medical University (HKSYDWLL2021025). A total of 20 4 to 5-week-old male Balb/c nude mice were purchased from SPF Biotechnology Co., Ltd (Beijing, China) and divided into four groups (n=5): the PBS group, the miR-192 group, the AG/PEI group, and the AG/PEI@miR-192 group. The HepG2 cell line was revived and cultured to the logarithmic growth phase. The cells were digested using trypsin and resuspended in saline after counting. The groin of nude mice was disinfected with alcohol cotton balls and 100–150 μl of HepG2 cells (1×10^7/100 μl) were inoculated subcutaneously into the mice to generate tumors. Each group of mice was separately administered 100 μl of PBS, along with untreated AG/PEI, water-soluble miR-192 at the same concentration as AG/PEI@miR-192, and AG/PEI@miR-192 itself, via *in situ* injection on a weekly basis. The tumor volume was observed during tumor development. The experiment was terminated 35 days after the inoculation, the mice were killed, tumors were excised and weighed, and tumor volumes were examined. $V=1/2 \times a \times b2$ (a is the long axis, b is the short axis).

Ethics approval. This study was approved by the Ethics Committee of The Third Affiliated Hospital of Wenzhou Medical University (HKSYDWLL2021025).

H&E staining. Tissues were embedded and cut into 4 μm thick sections using a microtome. After slide hydration, the slides are stained with Harris hematoxylin solution (Solarbio) for 5 min to remove excess hematoxylin. Subsequently, the slides are stained in eosin Y staining solution (Solarbio) for approximately 1 min, followed by rinsing with water. Prior to sealing the slides with neutral balsam, the slides undergo dehydration, and then they are observed and photographed under a microscope.

Statistical analysis. All experiments were carried out in triplicate and the data were expressed as mean ± SD. Statistical analyses were performed by SPSS 20.0 software (IBM, USA). Comparison between the two groups was performed with a two-tailed Student's t-test. Comparison between three or more groups was carried out using a one-way analysis of variance. A p-value <0.05 was considered statistically significant.

Results

Overexpressed miR-192 reduced the expression of CD90, EpCAM, and CD133. Each group of cells was divided into the NC group and the miR-192 group. As shown in Figure 1A, the expression of miR-192 in LO2, Bel-7402, and HepG2 in the miR-192 group was increased, indicating that miR-192 transfection was successful. As shown in Figure 1B, the expressions of surface markers CD90, EpCAM, and CD133 were decreased in Bel-7402 and HepG2 cell lines transfected with miR-192, as compared to the NC group, based on the results obtained from flow cytometry. To put

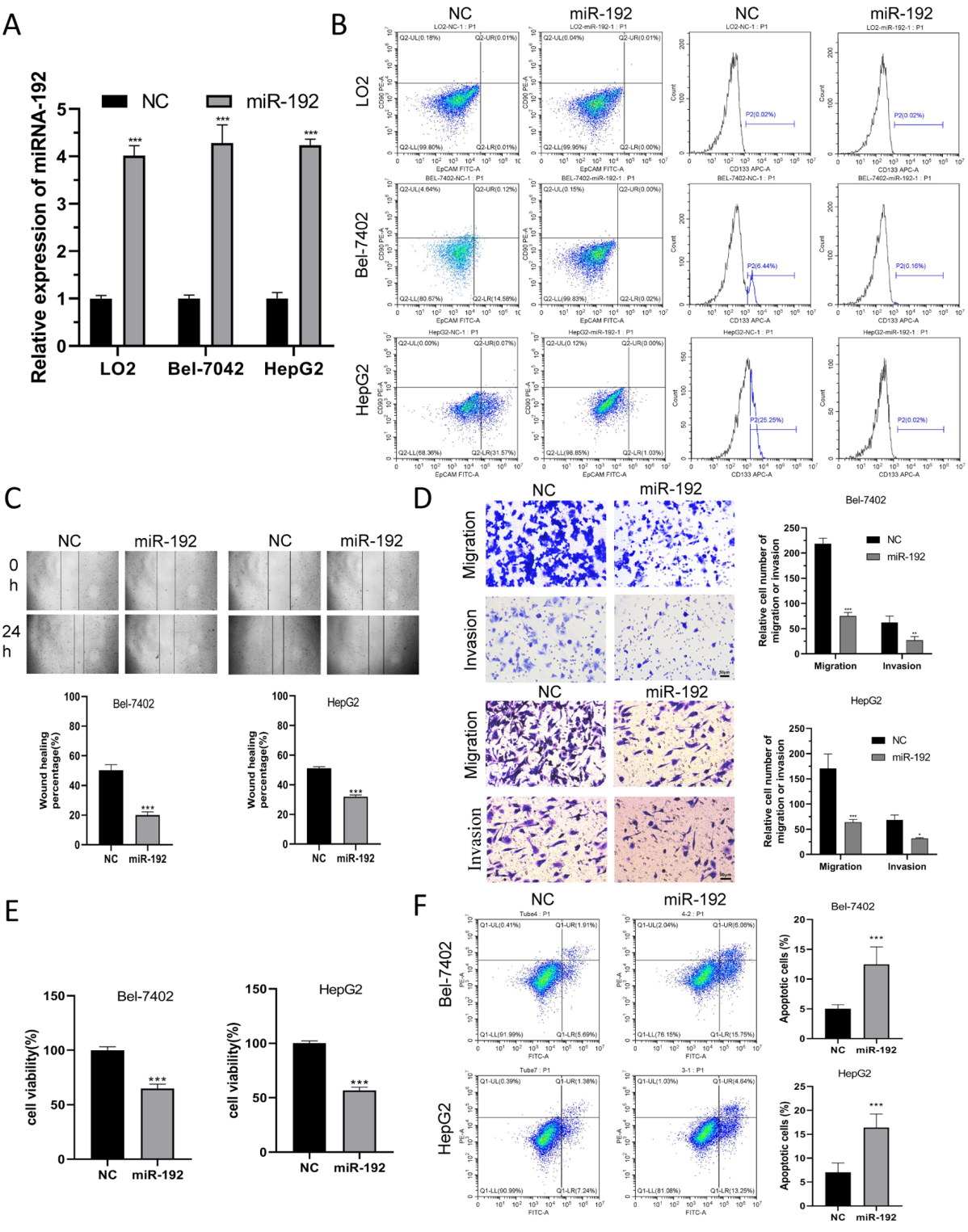

Figure 1. Validation of the roles of overexpressed miR-192 liver cancer cells. A) The overexpressed miR-192 cell line was constructed, including LO2 normal liver cell lines, Bel7042, and HepG2 hepatocellular carcinoma cell lines, and the expression of miR-192 was determined by PCR to verify the transfection efficiency. B) Flow cytometry was applied to determine the expression of HCC cell and normal liver cell surface markers CD90⁺, EpCAM⁺, and CD133⁺. C) Wound-healing assay was used to detect cell migration. D) The Transwell assay was performed to measure the migrative and invasive abilities of HCC cells. E) The CCK-8 assay was conducted to determine HCC cell proliferation. F) The apoptosis of HCC cells was detected using flow cytometry. Results are the mean ± SD for n=3 independent experiments for each group. ***p<0.001 vs. NC group

it another way, overexpression of miR-192 in normal cells does not affect the expression of surface markers, whereas changes in surface marker expression were observed in HCC cells. These findings indicate that miR-192 plays a role in the occurrence of HCC. (Figure 1B).

Overexpressed miR-192 inhibits HCC cell migration, invasion and proliferation, and promotes apoptosis. To explore the effects of miR-192 on HCC, wound-healing assay and Transwell assay were performed on HCC cells Bel-7402 and HepG2. As displayed in Figure 1C, cell migration was significantly impaired in the miR-192 groups compared to the negative controls. Additionally, the miR-192 groups had prominently diminished cell migrative and invasive abilities compared to the NC groups (Figure 1D). The CCK-8 assay indicated that the proliferative ability of HCC cells in the miR-192 groups was significantly lower than that of the NC groups (Figure 1E). Moreover, flow cytometry showed that apoptosis was more pronounced in the miR-192 groups compared to that in the NC groups, indicating that miR-192 promotes apoptosis in HCC cell lines (Figure 1F).

Overexpressed miR-192 inhibits the relative mRNA expression of β-catenin and c-Myc. To explore the mechanism by which miR-192 inhibits HCC, the levels of GS3Kβ, β-catenin, and c-Myc were determined by q-PCR. The results showed that the relative mRNA expression of β-catenin and c-Myc was remarkably reduced in the miR-192 groups

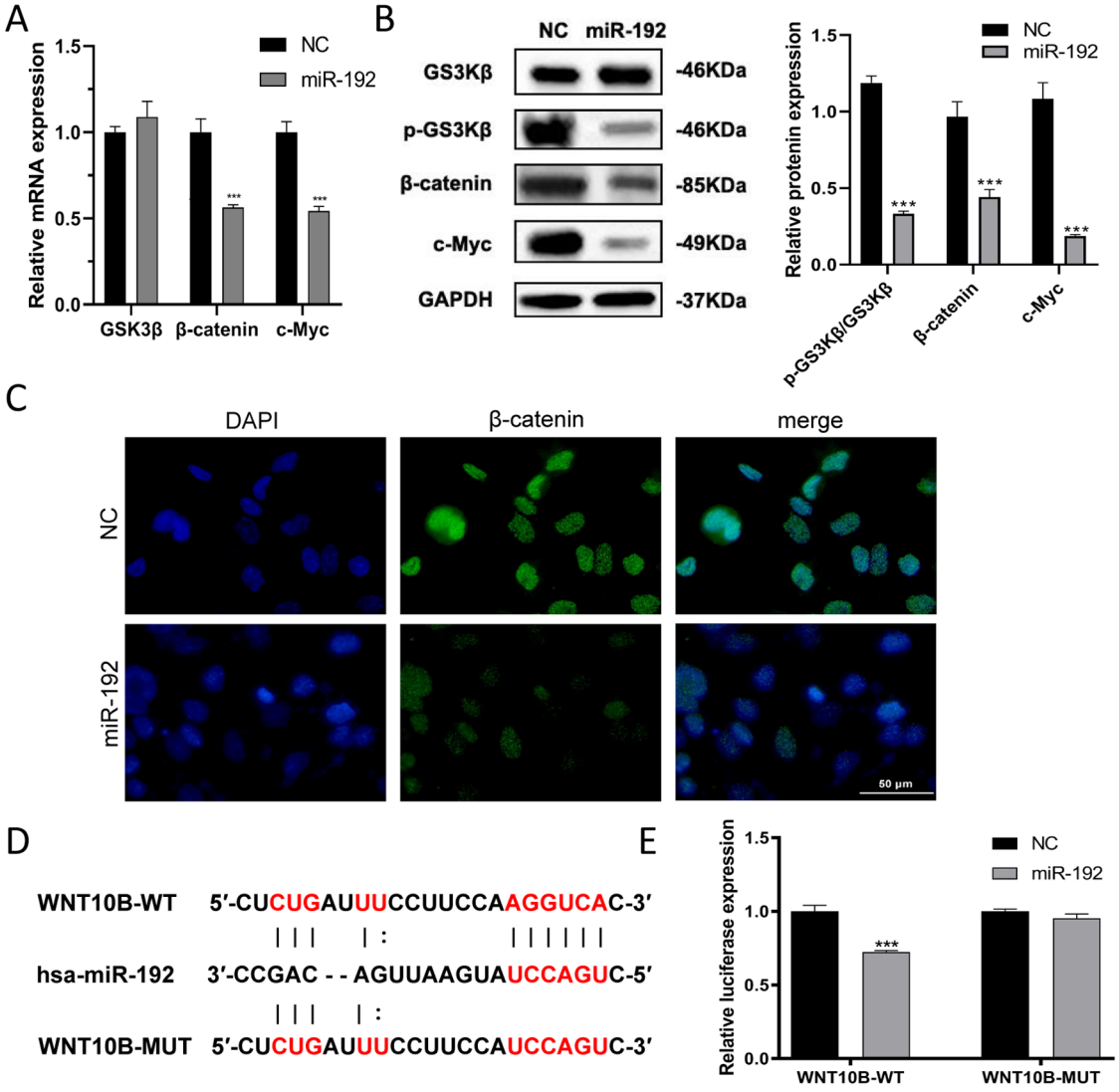

Figure 2. Association of miR-192 with GSK3β, Wnt/β-catenin, and c-Myc signaling pathways. A) The expression of GSK3β, β-catenin, and c-Myc in HepG2 cell lines was detected using q-PCR. B) The expression of p-GSK3β, GSK3β, β-catenin, and c-Myc in HepG2 cell lines was measured by western blot. C) Nuclear translocation of β-catenin was detected by immunofluorescence. D) Bioinformatics was used to predict the site where miR-192 binding to nucleic acid targets of GSK3β, Wnt/β-catenin, and c-Myc signaling pathways. E) The dual luciferase reporter assay was used to verify the interaction between miR-192 and GSK3β, Wnt/β-catenin, and c-Myc signaling target genes. Results are the mean ± SD for n=3 independent experiments for each group. ***p<0.001 vs. NC group

compared to that in the NC groups, while the mRNA expression of GSK3β was elevated but not statistically significant (Figure 2A). Western blot indicated that compared with the NC groups, the phosphorylation of GS3Kβ was decreased, and the protein expression of β-catenin and c-Myc was significantly decreased in the miR-192 groups (Figure 2B). Besides, immunofluorescence showed that the content of β-catenin in the miR-192 group was significantly lower than that in the NC group, indicating that miR-192 inhibited its entry into the nucleus (Figure 2C).

miR-192 interacted with the target gene of the Wnt signaling pathways. Bioinformatics website starBase (https://starbase.sysu.edu.cn) was used to predict the binding sites between miR-192 and the GSK3β, Wnt/β-catenin, and c-Myc pathways. The bioinformatics analysis manifested that WNT10B 3'-UTR might share the binding sites with miR-192 (Figure 2D). To explore the binding capability of WNT10B 3'-UTR and miR-192, a dual luciferase reporter assay was performed. The results revealed that co-transfection of miR-192 and WNT10B 3'-UTR plasmids reduced luciferase activity, while co-transfection of mutant WNT10B 3'-UTR plasmid and miR-192 restored luciferase activity, indicating that WNT10B is a direct target of miR-192 (Figure 2E).

AG/PEI nanohydrogel continuously delivered miR-192. After the successful preparation of the AG/PEI nanohydrogel, we left the hydrogel for 2,4, and 6 months. No precipitation or color change was found, indicating that the hydrogel had good stability (Figure 3A). The mean nanoparticle size was 109 nm (Figure 3B). The SEM images of the AG/PEI are illustrated in Figure 3C. For drug release, the cumulative release of miR-192 during the same time period was significantly higher than that of AG/PEI@miR-192, indicating that encapsulating miR-192 in the hydrogel could increase the stability of miR-192 and slow its release (Figure 3D). Furthermore, a CCK-8 assay was employed to detect the drug toxicity of AG/PEI, miR-192, and AG/PEI@miR-192. The results showed that the cytotoxicity of both the hydrogels and miR-192 at different concentrations on LO2 normal liver cell lines was low and the cell viability was greater than 90%, suggesting the good biocompatibility of the AG/PEI hydrogel (Figure 3E). In addition, cell toxicity experiments were conducted on HCC cell lines Bel-7402 and HepG2. Within the experimental concentration range, cell viability remained unchanged under the influence of AG/PEI, while as the concentration of miR-192-agomir gradually increased, cell viability significantly decreased as depicted in Figure 3F. This suggests that AG/PEI does not exhibit toxicity towards HCC cells, whereas AG/PEI@miR-192 can induce cytotoxic effects on HCC cells.

To verify the uptake of AG/PEI by cells, immunofluorescence was used. As shown in Figure 3F, after 2 h of incubation, the free FITC was in both the cytoplasm and nucleus, whereas in the AG/PEI@FITC group, the fluorescence was mainly in the cytoplasm and its fluorescence intensity was weaker than free FITC. After incubating for 6 h, the fluorescence intensity of FITC in the AG/PEI@FITC group was dramatically increased, indicating that more and more AG/PEI@FITC was internalized into the cells, suggesting that the drug-loaded nanohydrogel had a good drug sustained release effect.

AG/PEI@miR-192 suppressed tumor growth. To further detect the role of AG/PEI@miR-192, HE staining was applied. The results revealed that the tumor cells in the PBS group were closely arranged, the cell shape was complete, and the nucleus was visible, while the tumor tissue in the miR-192 group showed localized necrosis. The tumor cells in the AG/PEI group were tightly arranged, with intact cell shape and clear nuclei. However, tumor tissues in the AG/PEI@miR-192 group exhibited more extensive necrosis and loosened and ruptured cell arrangements, indicating that AG/PEI@miR-192 promoted cancer cell death (Figure 4A). Additionally, as shown in Figures 4B and 4C, tumors in the miR-192 group were regressed compared to those in the PBS group, and the inhibition of tumor growth was more pronounced after loading miR-192 to AG/PEI.

AG/PEI@miR-192 reduced the expression levels of GSK3β/Wnt/β-catenin/Tcf/Lef, and c-Myc. To validate the inhibitory effect of miR-192 on the tumor, the western blot and q-PCR were performed. Compared with the NC group, the miR-192 and AG/PEI@miR-192 groups had prominently lowered protein expression of β-catenin and c-Myc and its downstream target proteins Tcf7 and Lef1, and impeded phosphorylation of GSKβ (Figure 4D), while the relative mRNA expression of β-catenin, c-Myc, Tcf7, and Lef1 was reduced (Figure 4E), suggesting that miR-192 might hinder tumor cell growth by suppressing the activity of GSK3β/Wnt/β-catenin signaling pathway.

Discussion

In the present study, we demonstrated that miR-192 could inhibit HCC cell migration, invasion, and proliferation, and promotes cell apoptosis by suppressing GSK3β/Wnt/β-catenin pathway expression. Moreover, we established a nanohydrogel AG/PEI@miR-192 that could continuously deliver miR-192 in HCC cells and showed that AG/PEI@miR-192 significantly hindered tumor development.

HCC is one of the most common cancers worldwide and has extremely high incidence and mortality in Asia [19, 20]. miR-192 has been found to act as a tumor suppressor in a variety of cancers, including HCC. As one of the P53-induced miRNAs [21, 22], miR-192 is involved in cancer development and progression by targeting DHFR, TYMS, RB1, ZEB2, BCL2, and VEGFA [23–27]. However, the mechanism of miR-192 on HCC still requires further elucidation. In the present study, we constructed miR-192-overexpressing HCC cells and validated the functions of miR-192. The results revealed that the expression of surface markers was reduced in HCC cells transfected with miR-192, indicating a negative correlation between miR-192 and HCC cell growth. In addition, miR-192-overexpressing HCC cells had reduced

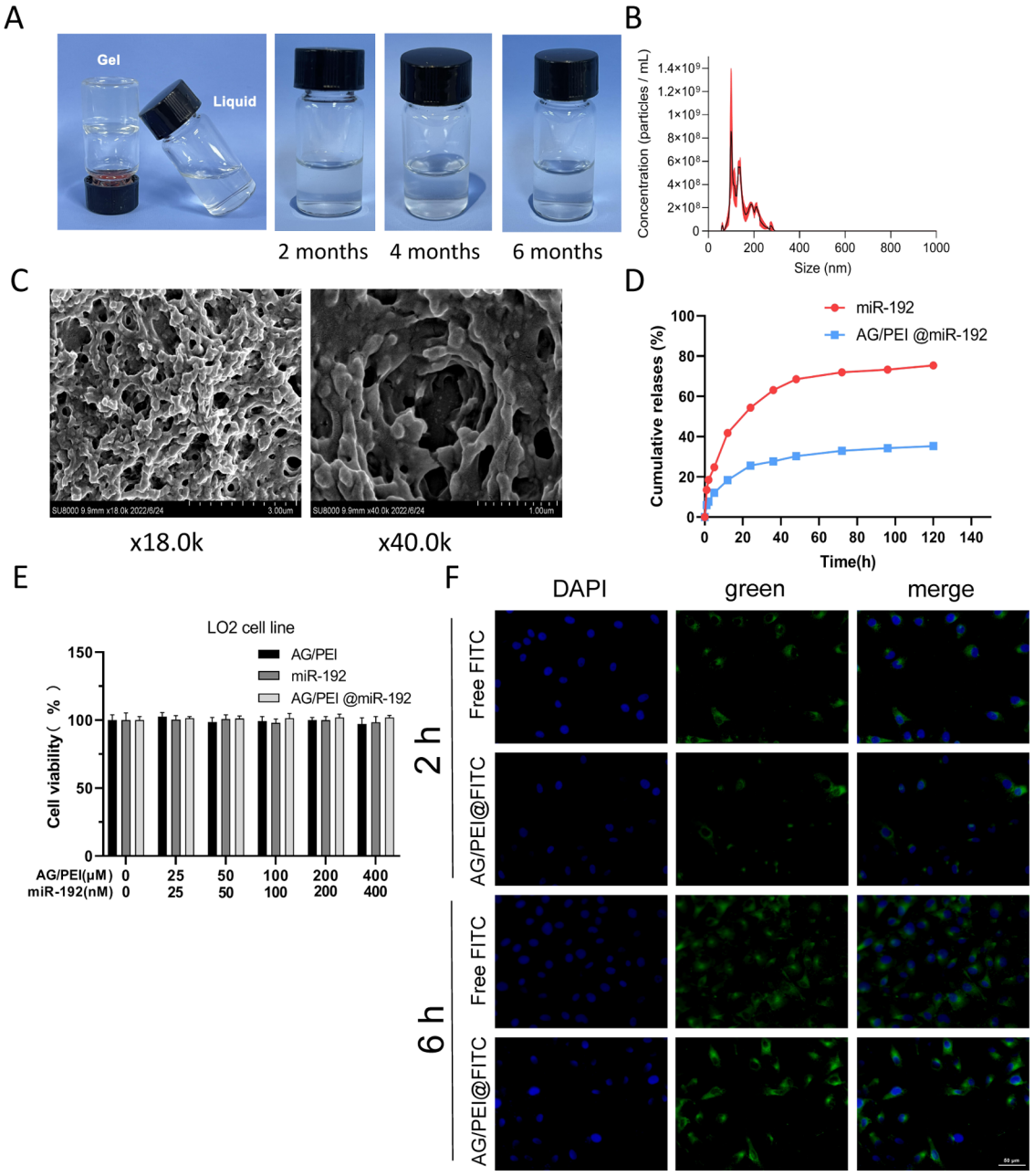

Figure 3. Validation of AG/PEI nanohydrogel for continuous delivery of miRNA-192. A) The AG/PEI nanohydrogel was left for 2, 4, and 6 months to observe its stability. B) Nanoparticle tracking analysis (NTA) was performed to detect the nanoparticle of AG/PEI hydrogel. C) Scanning electron microscope analysis was applied to observe the morphology and particle size of the AG/PEI@miR-192 nanohydrogel. D) The high-performance liquid chromatography (HPLC) method was carried out to determine the release characteristics of AG/PEI@miR-192. The CCK-8 assay was employed to detect the drug toxicity of AG/PEI nanogel and drug-loaded AG/PEI nanogel on E) LO2 normal liver cell lines and F) HCC cell lines, Bel7042 and HepG2 (n=3). G) Immunofluorescence was used to verify the uptake of miRNA by cells, where AG/PEI carrying FITC was used instead of AG/PEI@miR-192.

migrative, invasive, and proliferative abilities. miR-192-treated tumor tissues were locally necrotic and tumors were significantly smaller than those in the control groups, verifying that miR-192 inhibited the growth of HCC cells. Previous studies confirmed that the miR-3194-3p regulates the Wnt/β-catenin pathway [5], and GSK3 is a key signaling molecule in cancer as well as Wnt/β-catenin and regulates c-Myc [6]. Consistent with this, we found that overexpressing miR-192 reduced β-catenin and c-Myc expression. Also, we predicted the site where miR-192 binding to nucleic

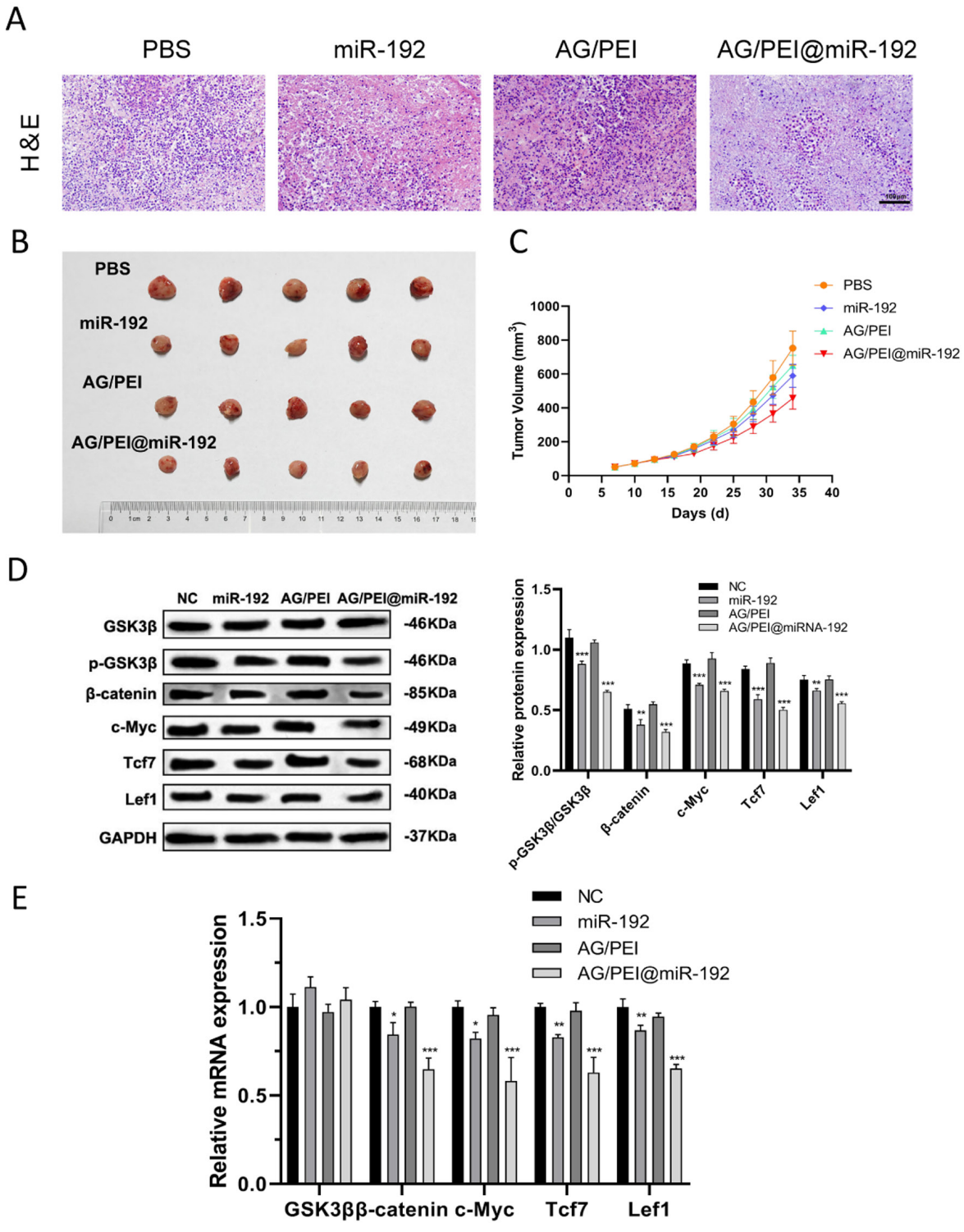

Figure 4. Construction of a nude mouse subcutaneous tumor model and validation of miR-192 function. Mice in each group received weekly in situ injections of 100 µl of PBS, untreated AG/PEI, water-soluble miR-192 (5 µM), and AG/PEI@miR-192 (5 µM). A) H&E staining was performed to observe the effect of miR-192 and AG/PEI@miR-192 on HCC tissues (arrow indicates necrotic cell, n=3). B) Images of excised tumors in different groups (n=5). C) The tumor volume in mice (n=5). D) The protein expression of GSK3β/Wnt/β-catenin/Tcf/Lef and c-Myc was measured using the western blot (n=3). E) The gene expression levels of GSK3β/Wnt/β-catenin/Tcf/Lef and c-Myc were determined by q-PCR (n=5). *p<0.05, **p<0.01, ***p<0.001 vs. NC group

acids targeting GSK3β, Wnt/β-catenin, and c-Myc signaling pathways, verified that miR-192 interacted with GSK3β, Wnt/β-catenin, and c-Myc signaling target genes, and demonstrated that miR-192 inhibited HCC by suppressing the GSK3β/Wnt/β-catenin pathway.

Although miRNAs can be used as markers for biological disease diagnosis, their poor stability *in vitro* and *in vivo*, nonspecific distribution, and off-target effects limit the use of therapeutic miRNAs in the clinical setting [28, 29]. Currently developed miRNA delivery vectors, such as viruses and liposomes, are biotoxic, cellular immunoreactive, and tumorigenic [30, 31]. Macrobiopolymer hydrogels like alginate and collagen, provide local and sustained delivery of small interfering RNAs (siRNAs) [32, 33]. Zhu et al. [34] produced a regenerative intra-articular microenvironment by delivering aging-related miR-29b-5p through stem cell homing hydrogels, thereby suppressing the abnormal metabolism of the cartilage matrix and promoting the repair of cartilage defects. Andrea et al. [35] enhanced cartilage regeneration from endogenous cells by constructing anti-miR-221 hydrogels. Cometa et al. [36] proposed a new electro-synthesized polyacrylic hydrogel film to prevent oral bacterial infections frequently related to oral and maxillofacial surgery. Qu et al. [17] constructed a pH-responsive self-healing injectable hydrogel based on N-carboxyethyl chitosan for HCC treatment and showed good performance. This study established AG/PEI hydrogel loading with miR-192 and investigated its delivery *in vitro* and *in vivo*. According to the results, the stability of the AG/PEI nanogel was good, and the release of miR-192 was slowed down after miR-192 was encapsulated in the hydrogel. Additionally, miR-192 or AG/PEI@miR-192 does not exhibit significant cytotoxicity towards normal liver cell lines, but it demonstrates significant cytotoxicity towards HCC cells. Moreover, AG/PEI shows its safety by not affecting the viability of both normal liver cell lines and HCC cell lines. The results of the *in vivo* experiments on tumor volume demonstrated that AG/PEI@miR-192 exhibited a more significant inhibitory effect on tumor growth compared to miR-192 alone, suggesting that AG/PEI@miR-192 had a more pronounced tumor suppression than miR-192. Meanwhile, the expression of β-catenin, c-Myc, and its downstream target proteins Tcf7 and Lef1 was diminished in the miR-192 and AG/PEI@miR-192 groups, and GSKβ phosphorylation was inhibited, further verifying that miR-192 might inhibit the growth of tumor cells by suppressing the activity of GSK3β/Wnt/β-catenin signaling pathway.

In conclusion, miR-192 impedes the migration, invasion, and proliferation of HCC cells, promotes apoptosis, and suppresses tumor cell growth by inhibiting the GSK3β/Wnt/β-catenin signaling pathway. This work established a hydrogel-based approach to deliver miR-192, and it represented good stability and sustained drug release, significantly hindering tumor cell growth, offering a theoretical basis and new therapeutic ideas for miRNA in the treatment of HCC.

Acknowledgments: This work was supported by the Ruian Science and Technology Bureau (MS2021010) and Wenzhou Science and Technology Bureau (Y20190684).

References

[1] CRAIG AJ, VON FELDEN J, GARCIA-LEZANA T, SARCOGNATO S, VILLANUEVA A. Tumour evolution in hepatocellular carcinoma. Nat Rev Gastroenterol Hepatol 2020; 17: 139–152. https://doi.org/10.1038/s41575-019-0229-4

[2] BROWN ZJ, GRETEN TF, HEINRICH B. Adjuvant Treatment of Hepatocellular Carcinoma: Prospect of Immunotherapy. Hepatology 2019; 70: 1437–1442. https://doi.org/10.1002/hep.30633

[3] SIMON J, OURO A, ALA-IBANIBO L, PRESA N, DELGADO T et al. Sphingolipids in Non-Alcoholic Fatty Liver Disease and Hepatocellular Carcinoma: Ceramide Turnover. Int J Mol Sci 2019; 21: 40. https://doi.org/10.3390/ijms21010040

[4] MACEK JILKOVA Z, ASPORD C, DECAENS T. Predictive Factors for Response to PD-1/PD-L1 Checkpoint Inhibition in the Field of Hepatocellular Carcinoma: Current Status and Challenges. Cancers 2019; 12: 2673. https://doi.org/10.3390/cancers11101554

[5] YAO B, LI Y, WANG L, CHEN T, NIU Y et al. MicroRNA-3194-3p inhibits metastasis and epithelial-mesenchymal transition of hepatocellular carcinoma by decreasing Wnt/β-catenin signaling through targeting BCL9. Artif Cells Nanomed Biotechnol 2019; 47: 3885–3895. https://doi.org/10.1080/21691401.2019.1670190

[6] GARCÍA DE HERREROS A, DUÑACH M. Intracellular Signals Activated by Canonical Wnt Ligands Independent of GSK3 Inhibition and β-Catenin Stabilization. Cells 2019; 8: 1148. https://doi.org/10.3390/cells8101148

[7] CHEN S, CAO Q, WEN W, WANG H. Targeted therapy for hepatocellular carcinoma: Challenges and opportunities. Cancer Lett 2019; 460: 1–9. https://doi.org/10.1016/j.canlet.2019.114428

[8] LI D, ZHANG J, LI J. Role of miRNA sponges in hepatocellular carcinoma. Clin Chim Acta 2020; 500: 10–19. https://doi.org/10.1016/j.cca.2019.09.013

[9] LI J, BAO H, HUANG Z, LIANG Z, WANG M et al. Little things with significant impact: miRNAs in hepatocellular carcinoma. Front Oncol 2023; 13: 1191070. https://doi.org/10.3389/fonc.2023.1191070

[10] PAN X, GUO J, LIU C, PAN Z, YANG Z et al. LncRNA HCG18 promotes osteosarcoma growth by enhanced aerobic glycolysis via the miR-365a-3p/PGK1 axis. Cell Mol Biol Lett 2022; 27: 5. https://doi.org/10.1186/s11658-021-00304-6

[11] HUA S, LEI L, DENG L, WENG X, LIU C et al. miR-139-5p inhibits aerobic glycolysis, cell proliferation, migration, and invasion in hepatocellular carcinoma via a reciprocal regulatory interaction with ETS1. Oncogene 2018; 37: 1624–1636. https://doi.org/10.1038/s41388-017-0057-3

[12] TEKSOY O, SAHINTURK V, CENGIZ M, INAL B, AYHANCI A. The Protective Effects of Silymarin on Thioacetamide-Induced Liver Damage: Measurement of miR-122, miR-192, and miR-194 Levels. Appl Biochem Biotechnol 2020; 191: 528–539. https://doi.org/10.1007/s12010-019-03177-w

[13] GU Y, WEI X, SUN Y, GAO H, ZHENG X et al. miR-192-5p Silencing by Genetic Aberrations Is a Key Event in Hepatocellular Carcinomas with Cancer Stem Cell Features. Cancer Res 2019; 79: 941–953. https://doi.org/10.1158/0008-5472.CAN-18-1675

[14] LIU XL, PAN Q, CAO HX, XIN FZ, ZHAO ZH et al. Lipotoxic Hepatocyte-Derived Exosomal MicroRNA 192-5p Activates Macrophages Through Rictor/Akt/Forkhead Box Transcription Factor O1 Signaling in Nonalcoholic Fatty Liver Disease. Hepatology 2020; 72: 454–469. https://doi.org/10.1002/hep.31050

[15] GU Y, JI F, LIU N, ZHAO Y, WEI X et al. Loss of miR-192-5p initiates a hyperglycolysis and stemness positive feedback in hepatocellular carcinoma. J Exp Clin Cancer Res 2020; 39: 268. https://doi.org/10.1186/s13046-020-01785-7

[16] YAN X, SUN T, SONG Y, PENG W, XU Y et al. In situ Thermal-Responsive Magnetic Hydrogel for Multidisciplinary Therapy of Hepatocellular Carcinoma. Nano Lett 2022; 22: 2251–2260. https://doi.org/10.1021/acs.nanolett.1c04413

[17] QU J, ZHAO X, MA PX, GUO B. pH-responsive self-healing injectable hydrogel based on N-carboxyethyl chitosan for hepatocellular carcinoma therapy. Acta Biomater 2017; 58: 168–180. https://doi.org/10.1016/j.actbio.2017.06.001

[18] LI S, LUO L, HE Y, LI R, XIANG Y et al. Dental pulp stem cell-derived exosomes alleviate cerebral ischaemia-reperfusion injury through suppressing inflammatory response. Cell Prolif 2021; 54: e13093. https://doi.org/10.1111/cpr.13093

[19] PARKIN DM, BRAY F, FERLAY J, PISANI P. Global Cancer Statistics, 2002. CA Cancer J Clin 2005; 55: 74–108. https://doi.org/10.3322/canjclin.55.2.74

[20] EL-SERAG HB, RUDOLPH KL. Hepatocellular carcinoma: epidemiology and molecular carcinogenesis. Gastroenterology 2007; 132: 2557–2576. https://doi.org/10.1053/j.gastro.2007.04.061

[21] BRAUN CJ, ZHANG X, SAVELYEVA I, WOLFF S, MOLL UM et al. p53-Responsive micrornas 192 and 215 are capable of inducing cell cycle arrest. Cancer Res 2008; 68: 10094-10104. https://doi.org/10.1158/0008-5472.CAN-08-1569

[22] GEORGES SA, BIERY MC, KIM SY, SCHELTER JM, GUO J et al. Coordinated regulation of cell cycle transcripts by p53-Inducible microRNAs, miR-192 and miR-215. Cancer Res 2008; 68: 10105–10112. https://doi.org/10.1158/0008-5472.CAN-08-1846

[23] BONI V, BITARTE N, CRISTOBAL I, ZARATE R, RODRIGUEZ J et al. miR-192/miR-215 influence 5-fluorouracil resistance through cell cycle-mediated mechanisms complementary to its post-transcriptional thymidilate synthase regulation. Mol Cancer Ther 2010; 9: 2265–2275. https://doi.org/10.1158/1535-7163.MCT-10-0061

[24] FENG S, CONG S, ZHANG X, BAO X, WANG W et al. MicroRNA-192 targeting retinoblastoma 1 inhibits cell proliferation and induces cell apoptosis in lung cancer cells. Nucleic Acids Res 2011; 39: 6669–6678. https://doi.org/10.1093/nar/gkr232

[25] GENG L, CHAUDHURI A, TALMON G, WISECARVER JL, ARE C et al. MicroRNA-192 suppresses liver metastasis of colon cancer. Oncogene 2014; 33: 5332–5340. https://doi.org/10.1038/onc.2013.478

[26] KIM T, VERONESE A, PICHIORRI F, LEE TJ, JEON YJ et al. p53 regulates epithelial-mesenchymal transition through microRNAs targeting ZEB1 and ZEB2. J Exp Med 2011; 208: 875–883. https://doi.org/10.1084/jem.20110235

[27] SONG B, WANG Y, KUDO K, GAVIN EJ, XI Y et al. miR-192 Regulates dihydrofolate reductase and cellular proliferation through the p53-microRNA circuit. Clin Cancer Res 2008; 14: 8080–8086. https://doi.org/10.1158/1078-0432.CCR-08-1422

[28] DU J, LI M, HUANG Q, LIU W, LI WQ et al. The critical role of microRNAs in stress response: Therapeutic prospect and limitation. Pharmacological Research 2019; 142: 294–302. https://doi.org/10.1016/j.phrs.2018.12.007

[29] HERRERA-CARRILLO E, LIU YP, BERKHOUT B. Improving miRNA Delivery by Optimizing miRNA Expression Cassettes in Diverse Virus Vectors. Hum Gene Ther Methods 2017; 28: 177–190. https://doi.org/10.1089/hgtb.2017.036

[30] CONDE J, OLIVA N, ATILANO M, SONG HS, ARTZI N. Self-assembled RNA-triple-helix hydrogel scaffold for microRNA modulation in the tumour microenvironment. Nat Mater 2016; 15: 353–363. https://doi.org/10.1038/nmat4497

[31] RESHKE R, TAYLOR JA, SAVARD A, GUO H, RHYM LH et al. Reduction of the therapeutic dose of silencing RNA by packaging it in extracellular vesicles via a pre-microRNA backbone. Nat Biomed Eng 2020; 4: 52–68. https://doi.org/10.1038/s41551-019-0502-4

[32] KREBS MD, JEON O, ALSBERG E. Localized and Sustained Delivery of Silencing RNA from Macroscopic Biopolymer Hydrogels. J Am Chem Soc 2009; 131: 9204–9206. https://doi.org/10.1021/ja9037615

[33] LUO L, HE Y, JIN L, ZHANG Y, GUASTALDI FP et al. Application of bioactive hydrogels combined with dental pulp stem cells for the repair of large gap peripheral nerve injuries. Bioact Mater 2021; 6: 638–654. https://doi.org/10.1016/j.bioactmat.2020.08.028

[34] ZHU J, YANG S, QI Y, GONG Z, YHANG H et al. Fang Stem cell-homing hydrogel-based miR-29b-5p delivery promotes cartilage regeneration by suppressing senescence in an osteoarthritis rat model. Sci Adv 2022; 8: eabk0011. https://doi.org/10.1126/sciadv.abk0011

[35] LOLLI A, SIVASUBRAMANIYAN K, VAINIERI ML, OIENI J, KOPS N et al. Hydrogel-based delivery of antimiR-221 enhances cartilage regeneration by endogenous cells. J Control Release 2019; 309: 220–230. https://doi.org/10.1016/j.jconrel.2019.07.040

[36] COMETA S, MATTIOLI-BELMONTE M, CAFAGNA D, IATTA R, CECI E et al. Antibiotic-modified hydrogel coatings on titanium dental implants. J Biol Regul Homeost Agents 2012; 26: 65–71.